Air Trenches for Sharp Silica Waveguide Bends

Miloš Popović, *Student Member, IEEE*, Kazumi Wada, Shoji Akiyama, Hermann A. Haus, *Life Fellow, IEEE*, *Fellow, OSA*, and Jürgen Michel

***Abstract*—Air trench structures for reduced-size bends in low-index contrast waveguides are proposed. To minimize junction loss, the structures are designed to provide adiabatic mode shaping between low- and high-index contrast regions, which is achieved by the introduction of "cladding tapers." Drastic reduction in effective bend radius is predicted. We present two-dimensional (2-D) finite-difference time-domain/effective index method simulations of bends in representative silica index contrasts. We also argue that substrate loss, while present, can be controlled with such air trenches and reduced to arbitrarily low levels limited only by fabrication capabilities. The required trench depth, given an acceptable substrate loss, is calculated in three dimensions using an approximate equivalent current sheet method and also by a numerical solver for full-vector leaky modes. A simple, compact waveguide T-splitter using air trench bends is presented.**

***Index Terms*—Air trench bend (ATB), cladding taper, enhanced lateral mode confinement, low-index contrast, sharp bend loss, silica waveguide.**

I. Introduction

LOW-INDEX contrast silica bench technology—referred to as planar lightwave circuit (PLC) or silicon optical bench (SiOB)—has gained widespread use in practice in the fabrication of passive integrated optical components by virtue of its use of well-tested integrated-circuit industry manufacturing processes and technology [1]. Large silica waveguide cross sections offer low fiber-to-chip coupling and propagation losses. A major drawback of SiOB technology is the relatively large component size, where a critical factor is the minimum waveguide bend radius. This radius is large—normally in the millimeters—in the low-index contrasts ($\Delta = 0.25\%$–1.5%) found in silica [1]. The low density of integration keeps production cost high and invites yield problems. On the other hand, high-index contrast, such as silicon-on-insulator (SOI)—while offering dense integration, poses challenges of fiber-to-chip insertion loss due to mode shape mismatch and misalignment, scattering loss, and sensitivity to other fabrication defects and tolerances, as well as fabrication processing challenges.

Manuscript received November 5, 2001; revised June 12, 2002. This work was supported in part by the Materials Research Science & Engineering Centers (MRSEC) Program of the National Science Foundation under Award DMR 98-08941, by a Natural Sciences and Engineering Research Council (NSERC) of Canada PGS-A scholarship, and by a National Partnership for Advanced Computing Infrastructure (NPACI) supercomputer allocation.

M. Popović and H. A. Haus are with the Research Laboratory of Electronics, Massachusetts Institute of Technology, Cambridge, MA 02139 USA (e-mail: milos@mit.edu).

K. Wada, S. Akiyama, and J. Michel are with the Department of Materials Science and Engineering, Massachusetts Institute of Technology, Cambridge, MA 02139 USA.

Digital Object Identifier 10.1109/JLT.2002.802230

A technology that allows a drastic reduction in the bending radius would overcome one of silica's major obstacles to attaining truly large-scale optical integration. We propose a scheme using air trenches to provide locally enhanced lateral mode confinement. We use adiabatic tapering to avoid abrupt junction-induced mode mismatch and Fresnel reflection in order to miniaturize optical waveguide bends while preserving low-loss performance [13].

In the last 30 years, much attention has been devoted to the design of waveguide bends and the proper analysis of their losses [2]–[5], [11], including the use of air trenches. More recent contributions include "deep etching" in InP-ridge waveguide bends [6], and a proposal of more unconventional, low-Q cavity bends in high-index contrast, such as SOI [7].

Air trenches have been proposed for suppressing bend radiation in several ways [6], [10]. When they are used to enhance lateral mode confinement, mode mismatch-induced junction loss is incurred at points of abrupt change in refractive index and/or cross-sectional waveguide geometry, limiting the success of the approach [6], particularly in low-index contrast. To our knowledge, no attempt has been made to use air trenches to improve bending loss in low-index contrast by properly addressing the mode-mismatch issue introduced by the present air trench, to produce small, low-loss bends. We use judiciously placed air trenches for sharp bending with adiabatic transition to mitigate junction loss. It is generally recognized that adiabatic mode shaping results in low-loss tapers and directional couplers (e.g., see [8]).

In this paper, we introduce a pair of "cladding tapers" as an integral part of the etched air trench at the bend (Fig. 1) in order to provide fast mode transition to and from the high-index contrast trench region with low radiation loss and low reflection. The main high-index contrast region in this case contains the waveguide bend. The result is a reduction in bending radius by a factor of 10–1000 and in total bend structure edge length by a factor of 4–60. The theoretical justification for the proposed idea is presented primarily in terms of two-dimensional (2-D) finite-difference time-domain (FDTD) simulations of air trench bends (ATBs) with index contrast between $\Delta = 0.25\%$ and $\Delta = 7\%$.

In Section II, we describe the ways in which air trenches have been used in prior work and justify our approach to the problem in low-index contrast. In Section III, we first show the performance and physical size of a regular waveguide bend, without air trenches, for a set of chosen index contrasts. We then describe the method used to produce the ATB structure designs, and, in Section IV, we show 2-D simulation results, including dimensions and performance. In Section V, we discuss mode confinement issues that are important in properly accounting for

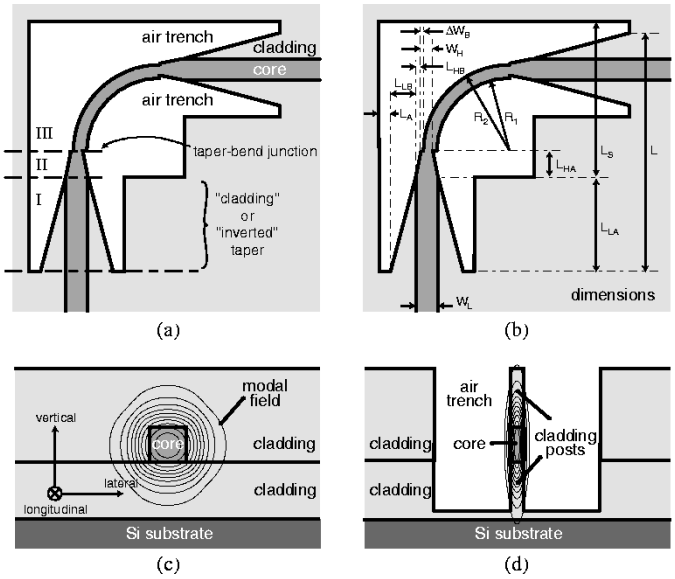

Fig. 1. ATB structure schematic: (a) Labeled plan view. (b) Dimensioned plan view. (c) Cross-sectional views in the low-index. (d) Air trench regions. Contour plots representative of the dominant modal electric-field component are superimposed on the cross sections (not to scale).

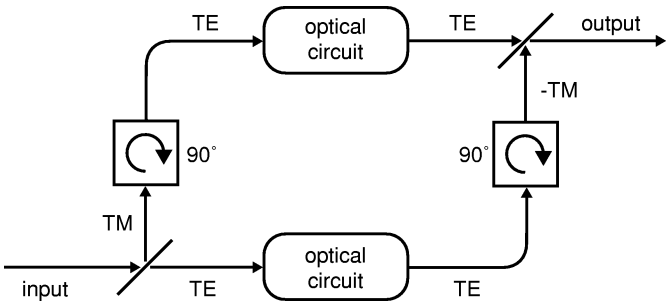

Fig. 2. Optical circuit layout for polarization-independent operation using polarization-dependent components and polarization splitters and rotators.

the third dimension in the simulations, and we address substrate leakage and polarization dependence. We calculate the minimum air trench depth for tolerable substrate loss. A full-vector finite-difference numerical mode solver for a 2-D cross-section leaky waveguide is used to verify the approximate computations of substrate losses of the proposed waveguides. Finally, in Section VI, a waveguide T-splitter using ATBs is shown as an example of a simple compound device utilizing the bends.

We state here that the polarization sensitivity of these structures was not a design consideration because it is recognized as being inevitably poor, as is generally found in high-index contrast and especially in a structure with high cross-sectional asymmetry along the principal polarization directions, such as with the structures presented here. We used the vertical (out-of-the-wafer plane, Fig. 1) electric-field polarization for our designs. We propose that the orders-of-magnitude chip area savings offered by this approach warrants the making of two identical optical circuits, one for each polarization. The signal polarizations may then be split and one rotated such that both are processed by identical circuits before being recombined in a similar way at the output, as shown in Fig. 2.

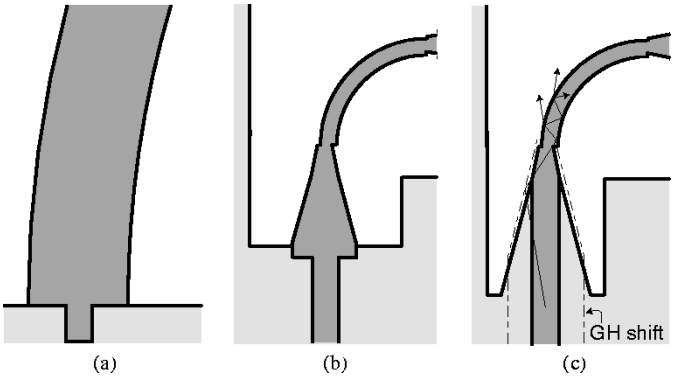

Fig. 3. Incorporating an air trench into a waveguide bend using (a) an abrupt junction, (b) an abrupt junction followed by a taper, and (c) the proposed adiabatic cladding taper. The bend radius is junction loss limited in (a), but curvature loss limited in (b) and (c). Junction loss is present in (a) and (b), but is virtually eliminated in (c). The dash-dot line in (c) shows a local Goos–Hänschen shift and a ray trace of coupling to the bend mode (not to scale).

II. Air Trenches for Enhanced Lateral Confinement

The use of air trenches for sharp bending radii, in addition to being an obvious and integral part of air-clad high-index contrast waveguides (e.g., SOI), has been discussed previously in the context of optical fiber, slab [10], and ridge waveguide bend loss [6]. In the former case, the trench is placed away from the core with the intention of extending the reach of the evanescent part of the leaky-mode (LM) field. The "radiation caustic" is pushed radially outward, without significantly altering the shape of the LM [10]. In the latter case, trenches were "deep etched" immediately next to the core of InP/InGaAsP-ridge waveguides, providing higher lateral mode confinement at the expense of junction loss [6].

In typical silica index contrasts, the abrupt junction loss at the interface between the standard waveguide and the trench region [as in Fig. 3(a)] becomes intolerable for any bend radii small enough to make the air trench useful in reducing size. This demands our use of an adiabatic taper. For clarity, we will briefly illustrate the argument for the slab (2-D) case. In a straight-to-straight waveguide junction with a silica input waveguide constrained to be single mode, by varying the trench-clad output waveguide's core width, mode distributions can be optimally matched. A surprisingly low loss can be obtained, <0.1 dB, even for fiberlike index contrasts in the input waveguide $(\Delta \sim 0.25\%)$. This optimum loss occurs for a wide, greatly overmoded trench waveguide, with the fundamental mode width essentially determined by the core width [Fig. 3(a)]. When the trench waveguide is curved, however, for small radii, the mode width is not determined by the waveguide width, but rather, by the bend radius (whispering-gallery regime, e.g., see [12]). The field distribution width of the LM becomes narrower for smaller bends, setting a lower limit on the bend radius compatible with the above minimized junction loss, e.g., 15 mm for $\Delta = 0.1\%$ (based only on matching the modal width, even without accounting for qualitative mode shape differences). In the low-index contrast input waveguide, the field distribution of the fundamental mode has a minimum width determined by the index contrast and, thus, *a priori* cannot be matched well to the first LM of arbitrarily tight bend radii. To produce small bend radii, it is necessary to provide a low-loss mechanism to

compress the input mode. We propose the use of an adiabatic "cladding taper" [Figs. 1 and 3(c)]. Constrained only by the overall loss of the structure, these tapers allow reduction of the bend radius in the trench region to the point where it is limited by bending loss, rather than the modal distribution width required for acceptable junction loss.

A progression from an abrupt junction to a cladding taper is illustrated in Fig. 3. As argued above, an abrupt junction [Fig. 3(a)] requires a large bending radius. A taper after the abrupt junction can be used to compress the mode so that a tighter bend radius can be used [Fig. 3(b)]. However, a more natural way to build the transition is by introducing the taper as a slow perturbation of the waveguide's index profile, as shown in Fig. 3(c). This eliminates the reduced but present Fresnel reflection at the junction of Fig. 3(b) and requires a less abrupt modification of the propagating mode while providing equally fast tapering. The proposed air trench is introduced gradually (in the form of the aforementioned cladding taper) and away from the core, where the field is small, in order to allow an adiabatic evolution of the mode to a shape better matched to the leaky bend mode used in the high-index bend region.

In the presented examples, we use a square cross-section, low-index contrast buried waveguide with a good match to the fiber mode for inherently low-loss fiber-chip coupling. We employ air trenches surrounding (and etched through part of) the core region to provide high lateral confinement in the plane, while leaving the mode weakly confined in the vertical direction [see mode contour plots in Fig. 1(c) and (d)]. By having air in place of much of the cladding material near the core, the fundamental mode has a lower modal index than the cladding index. At first glance, this might suggest inevitable leakage to the cladding in the trench region, but this is in fact not a necessary consequence. In order to curb leakage to the substrate and also prevent the evanescent tails of the field in the vertical direction from radiating sideways in a bend, the air trench is etched well below the core [Fig. 1(d)]. As discussed in Section V, etching below the core allows reduction of substrate loss to arbitrarily low levels, as limited only by concerns with fabrication of a high-aspect ratio structure.

We analyze the bend in the trench region using some standard semianalytic tools [2]–[5], [11]. The trench tapers are designed using some initial ray optics intuition and iteratively optimized through simulations (alone or as part of the complete bend structure) using FDTD.

III. Air Trench Bend: Bend and Taper Design Method

Optimization for minimum size given a required transmission efficiency of a device, such as the present ATB—consisting of a bend and two tapers—is a complex problem where variation in the parameters of one subcomponent in general influences all others. For a simpler approach, we choose a bend using some simple criteria and then optimize the taper parameters with respect to the chosen bend design without recursion. In our higher index examples, where the bend accounts for a significant part of the structure size, we choose the minimum bend radius meeting curvature-loss requirements. In lower index examples, where the bend radius contributes little to overall structure size, we oversize the bend radius in order to lower the taper-bend junction loss [Fig. 1(a)]. For loss analysis and design, we separate the structure into its two constituent tapers and the high-index bend between them.

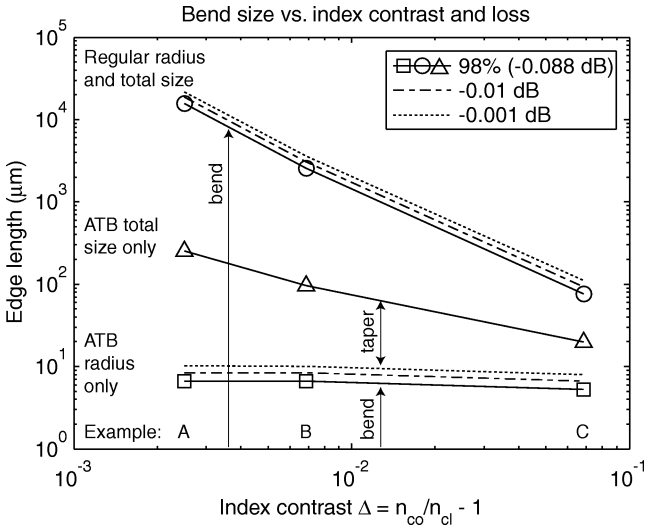

Fig. 4. Bend (radius and "total box") size for regular waveguide bends and ATBs, showing improvement in size for the case of 0.1-dB loss. It is also shown that, on this scale of size variation, the relative change in radius is small for 0.01- and 0.001-dB loss.

A. Regular and ATB Loss

In a conventional curved waveguide, bending loss is minimized by coupling to the lowest order LM [2]–[5], [11]. The total loss in a corner bend comes from the bending loss of the chosen LM and from junction loss at the interfaces between the straight and bent waveguides. In the ATB, additional loss is incurred by propagation through each cladding taper and at the junction where each taper meets the low-index contrast waveguide (Fig. 1). The latter is primarily related to the change of phase front curvature.

Furthermore, in regular waveguide bends, the radius and width of the bend and its axial offset with respect to the straight waveguides are free parameters, but where single-mode waveguides are used, the width of the straight waveguide is generally fixed. (Tapering out to a larger width at the junction is also possible, but not desirable, since mode-matching can instead be accomplished by reducing the bend radius. Reduction of the bend radius is limited at some point by bend loss.) In the ATB case, the waveguide width at the taper side of the taper-bend junction [W_H, Fig. 1(b)] is also a free parameter and need not be constrained by single-modedness in the local normal-mode sense. This is because the input single-mode waveguide is much wider than that in the high-index contrast bend region [$W_L \gg W_{H,\mathrm{singlemode}}$, Fig. 1(b)]; a wider taper output (W_H) allows for a less steep (and thus, more efficient) taper.

First, we consider bending loss, namely, in regular waveguide bends without an air trench, or in case of the ATB, we consider the curvature loss in the bend-containing trench region. Radiation loss in regular bends and ATBs is evaluated numerically according to the approaches in [4] and [5] after the customary conformal transformation for bent waveguides [3]. Bends are designed for an overall 98% transmission or ~0.1-dB loss per right-angle bend, and the bend parameters are shown in Fig. 4 and Tables I and II for three chosen index contrasts,

TABLE I
REGULAR AND ATB RADII AND TOTAL SIZES FOR 98% TRANSMISSION

Property		Example A	Example B	Example C	units
Index	Contrast (Δ)	0.25	0.68	6.85	%
Regular Bend	Radius	15700	2565	76	μm
	Total Size[a]	15708	2570	78	μm
Air Trench Bend	Radius	15.35	9.25	7.25	μm
	Total Size[a]	252.60	95.85	19.75	μm
Size Reduction	by Length	62	27	4	
	by Area	3867	719	16	

[a] Edge length of a box enclosing the entire bend structure and accommodating >99.9% of the input and output mode power. The minimum bend size possible is a square with an edge equal to this 99.9% mode width.

TABLE II
ATB LOSS BUDGET

Property		Example A	Example B	Example C	units
Index Contrast (Δ)		0.25	0.68	6.85	%
ATB Losses	Bending	0.0020	0.0024	0.0023	dB/90°
	Taper-Bend Junction	0.0090	0.0355	0.0394	dB/jctn
	Taper	0.0232	0.0187	0.0089	dB/taper
	Total Loss[a]	0.074[b]	0.061	0.052	dB
	Transmission	98.3[b]	98.6	98.8	%

[a] Total loss is due to 2 tapers, 2 junctions and 90° of bending. Estimated individual losses do not exactly add to equal the total loss, because the latter is the result of a simulation of the entire structure and as such is more accurate. Junction loss at the interface between the low index waveguide and the cladding taper is deemed negligible and ignored.

[b] Loss from 180° ATB (note that bending loss is only 0.002 dB/90°).

including (for ATBs) separately calculated proportions of loss attributed to junction mode mismatch and bending radiation. The regular bend is constrained to have single-mode input and output waveguides, while the ATB bend region is only constrained to have them smaller than the low-index waveguide ($W_H < W_L$)—which effectively presents no constraint. The bending loss is evaluated in the usual way by solving for the complex propagation constant of the lowest order LM using either the linearized, conformally transformed dielectric constant profile, where the modal field is expressed in terms of Airy functions [4], [5], or the Wentzel–Kramers–Brillouin (WKB) method for very low loss bends [12]. Where both can be used, the two approaches yield comparable numbers.

The second contributor to loss in a finite-angle bend is junction loss at the start and end points. Junction loss between two straight slab waveguides is determined by matching guided and radiation modes at the junction, using a scattering matrix approach (e.g., see [12]). For a straight-to-bend junction, and neglecting scattering into reflected (backward) radiation modes, we obtain a simple expression that includes the overlap integral of the leaky bend mode field computed previously with the mode of the straight waveguide. The appropriate expression for power coupling efficiency at a straight-to-bent slab junction is given by

$$\eta = \frac{\beta_2}{\beta_1}\left(\frac{2\beta_1}{\beta_2+\beta_1\frac{\langle E_2\,|\,E_2\rangle}{\left\langle E_2\left|\frac{R}{r}\right|E_2\right\rangle}}\right)^2 \frac{\langle E_2\,|\,E_1\rangle^2}{\left\langle E_2\left|\frac{R}{r}\right|E_2\right\rangle\langle E_1\,|\,E_1\rangle} \quad (1)$$

resulting in a junction loss of $L_J = -10\log\eta$ (dB). Here, $\beta_{1,2}$ are propagation constants, $E_{1,2}$ are the modal electric-field amplitudes of the two waveguides at the junction, R is the bend radius, and r is the radial coordinate that is identical to the transverse x coordinate of the straight waveguide along the junction. The one-dimensional (1-D) overlap integral in this TE slab waveguide case is, for example,

$$\left\langle E_2\left|\frac{R}{r}\right|E_1\right\rangle = \int_0^{R_{\text{caustic}}} E_2^*(r)\cdot\frac{R}{r}\cdot E_1(x)\,dx\Bigg|_{r=x} \quad (2)$$

and simplifies to the case for straight waveguides for $R \to \infty$, where $R/r \to 1$ over the range of r values where the integrand (modal field) significantly contributes to the integral. The integral is terminated at the radiation caustic R_{caustic}. For the straight slab junction case, FDTD simulations were done to check on the validity of ignoring reflected radiation modes, which confirmed a high accuracy for low junction losses of <1 dB. When the input waveguide is of low-index contrast, such as the case considered here, loss in regular waveguide bends is dominated by bending loss, and junction loss can be ignored. For trench-clad bends (the bend region of ATBs), junction loss must be incorporated into the loss figure.

B. Cladding Tapers

In the case of the ATB, the purpose of our cladding taper is to adiabatically shape the fundamental mode of the low-index contrast input waveguide [at the input of Section I, Fig. 1(a)] to the shape of the fundamental mode, in the local normal mode sense, of the high-index contrast (air trench-clad) output [at the output of Section II, Fig. 1(a)]. In low-index contrast, this output mode can be much smaller than the minimum possible width of the input waveguide mode. The output waveguide width is fixed by the bend design from optimization of the trench region's taper-bend junction loss. For simplicity, the cladding tapers considered are piecewise linear, but it is recognized that because of the need for adiabatic shaping of phase front curvature in addition to mode shape, the optimal taper of this kind will have a more complex shape. For our analysis, a cladding taper with a constant width core is broken up lengthwise into two distinct regions with piecewise linear tapers: one where air surrounds the core and cladding [the outer, "cladding" taper—I in Fig. 1(a)] and one where air surrounds the core directly [the inner, "core" taper—II in Fig. 1(a), which transitions to the bend, III].

Optimization of the taper is dealt with in a less analytic manner than the bend due to its geometric complexity. The initial estimate for the tapering angle of each of the inner and outer tapers is obtained from considering the ray-optical description of the input and output fundamental modes. Ray angles from the plane- wave description of input and output (local normal) modes are used in conjunction with an extrapolated Goos–Hänschen shift to determine a taper angle that would guide the input ray directly into the output ray with minimal loss (i.e., in a "single bounce"), as illustrated in Fig. 3(c). While this is a highly simplistic picture, it is useful in providing an initial estimate. The refining of the taper parameters requires few steps and is done here by hand, via iterated

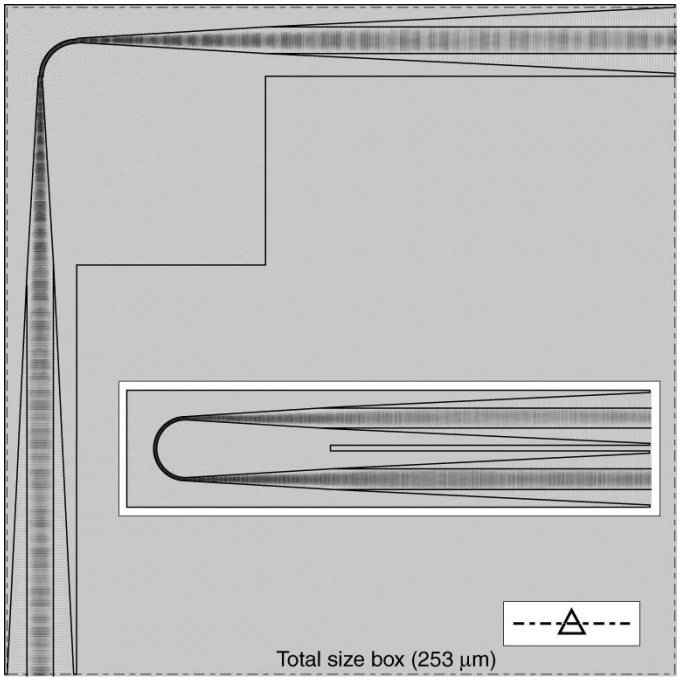

Fig. 5. Example A. Dominant electric-field plot from FDTD simulation, and the total size box (dash-dot square). Inset shows field plot of simulation used for throughput efficiency lower bound (180° bend) due to simulation size constraints. Key in lower right corner refers to transmission data in Fig. 8.

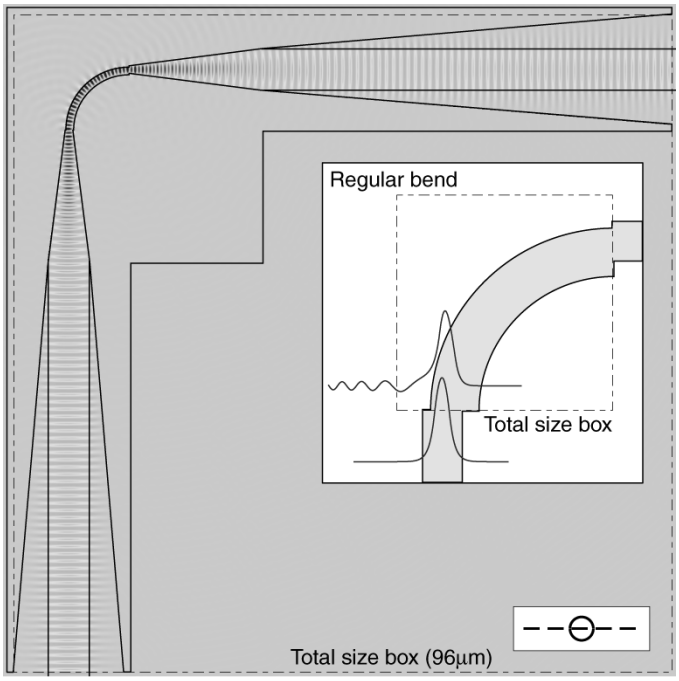

Fig. 6. Example B. Dominant electric-field plot from FDTD simulation. Total size box is outlined (dash-dot square) for ATB and for a regular bend (inset) for reference. Key in lower right corner refers to transmission data in Fig. 8.

computer simulation. The tapers are finally characterized by full 2-D FDTD simulations, which, while computationally costly, should provide an accurate estimate of performance. Results of individual taper efficiency are listed in Table II, with equal throughput efficiency in either direction, as required by reciprocity.

We split the total loss between the cladding tapers and the trench bend in such a way that the tapers (which dominate the size of lower index contrast structures—Figs. 5–7) carry a larger part of the losses in order to minimize total structure size. Bend-region loss can be much improved with small radius increases (see Fig. 4). In lower index contrast, where bends constitute a small part of the ATB structure, radius-sensitive bend loss can be practically removed and taper-bend junction loss reduced with a small radius increase, then redistributed among the tapers to reduce overall structure size.

IV. ATB Examples With 2-D Simulation Results

We present 2-D simulation results for several example ATBs, designed in the manner described above, chosen to demonstrate the proposed idea and illustrate its effectiveness in reducing bend size in various index contrasts. Examples A–C range in index contrast from 0.25% to 7%, where the last example is outside the range of typical index contrasts found in silica waveguides ($\Delta < 1.5\%$) [1]. It was used as our first structure because of its small size in terms of wavelengths and, thus, short simulation time. Refractive indexes and dimensions for the example structures are given in Table III. The refractive indexes that are chosen for all examples are ones that could be produced in SiO_xN_y-core/SiO_2-cladding waveguides. SiON has an index tunability over the range of 1.45–1.96 [15].

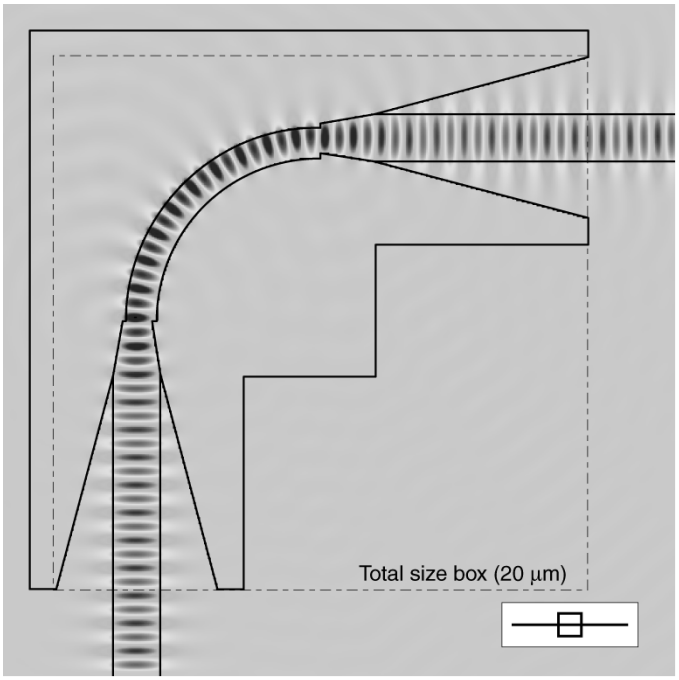

Fig. 7. Example C. Dominant electric-field plot from FDTD simulation. Total size box shown for reference (dash-dot square). The key in the lower right corner refers to transmission data in Fig. 8.

A. FDTD Simulation Setup

The ATB structure is reduced to two dimensions for simulation by using the effective index method (EIM) with perturbative correction [14], which works well in spite of the square cross-sectional geometry of the waveguides and high aspect ratio of the trench (see Section V). In applying the EIM, it is assumed that the mode is always well confined if

TABLE III
ATB STRUCTURE DIMENSIONS

	Property	Example A	Example B	Example C	units
Refractive Index	Contrast (Δ)	0.25	0.68	6.85	%
	Core	1.46365	1.47	1.56	
	Cladding	1.46	1.46	1.46	
Dimensions	R_1 Inner Radius	14.20	8.10	6.10	μm
	R_2 Outer Radius	15.35	9.25	7.25	μm
	W_L Big Waveguide Width	10.05	6.05	1.75	μm
	W_H Small Waveguide Width	1.05	1.05	1.05	μm
	ΔW_B Bend Offset	0.00	0.10	0.10	μm
	L_{HA} Hi-Δ Air Triangle Length	70.20	19.00	2.05	μm
	L_{HB} Hi-Δ Air Triangle Width	4.50	2.50	0.35	μm
	L_{LA} Lo-Δ Air Triangle Length	155.00	60.00	7.90	μm
	L_{LB} Lo-Δ Air Triangle Width	7.55	5.00	2.10	μm
	L_S Air Square Edge Length[a]	98.60	36.85	12.85	μm
	L_A Air Buffer Width	1.00	1.00	1.00	μm
	L Total Structure Edge Size	252.60	95.85	19.75	μm

[a] The "air square" is not a useful part of the ATB, but is an artifact of generating the structure index profile for FDTD simulation. It aligns to the boundary between the core taper and the cladding taper.

TABLE IV
COMPARISON OF EFFECTIVE INDEX METHOD AND VECTOR MODE SOLVER

Property	Method	Polarization	Example A	Example B	Example C	units
Index Contrast (Δ)			0.25	0.68	6.85	%
Silica Guide Modal Index	EIM	quasi-TE	1.4619	1.4651	1.5054	
	Vectorial	both	1.4620	1.4654	1.5077	
Air Trench Modal Index[a]	EIM	quasi-TE	1.3820	1.3867	1.4494	
	Vectorial	quasi-TE	1.3782	1.3828	1.4454	
	Mode Solver	quasi-TM	1.3455	1.3498	1.4122	

[a] Modal index of a straight air trench waveguide mode, not that of a bend.

the waveguide is straight, and that substrate (or bulk cladding) leakage beneath the air trench is negligible. Thus, we concern ourselves only with loss due to bending in the plane. The core effective index is obtained by the traditional EIM, while for the cladding, it was obtained by perturbation of the propagation constant, assuming the same shape of mode field as in the core [14].

FDTD results for transmission loss are obtained by launching a short pulse (on the order of 50 fs) into the input waveguide with enough spectral width to span the wavelength spectrum of interest. A discretization of ∼20 points per wavelength is used, with the perfectly matched layer (PML) absorbing boundary condition imposed on the edges of the 2-D computational domain. The total power flux through the output waveguide cross-sectional plane is monitored, and an overlap integral with the fundamental mode of the waveguide is carried out to obtain transmission efficiency at the central wavelength (and, similarly, for reflection back to the input waveguide). A simulation is terminated once the pulse has left the computational domain and all fields have sufficiently died out.

B. Regular Bend Results

Radiation losses of regular waveguide bends (without air trenches) are evaluated using standard tools for 2-D (bent slab) waveguides mentioned previously, making use of the EIM to "collapse" the third dimension. Since their loss per wavelength along the propagation direction is very low, FDTD would be too computationally costly (and perhaps inaccurate) for such structures. The values obtained for the regular bend radius without an air trench—as required for a transmission of 98% or loss of 0.1 dB/90°—are shown in Table I (using the effective indexes from Table IV).

C. ATB Results

ATB structures corresponding to each of these regular bends are then designed and simulated using 2-D FDTD (vertical electric or TE-like polarization). Contrary to convention, we refer to the polarization of the mode with a vertical dominant electric-field component (E_y) as TE-like or quasi-TE. We do so because this mode in the trench region looks TE-like, and for $\Delta \to 0$ approaches the slab waveguide TE mode. In the square cross-section low-index input waveguide, the modes are degenerate, and the labeling does not matter. Figs. 5–7 are plan view plots of the electric-field amplitude superimposed on the outline of the structure. The absence of obvious radiation gives qualitative evidence that these bends exhibit low loss. The new bend radii and total or "box" edge lengths, including tapers (i.e., the effective radii), are listed in Table I alongside regular bend data and show drastic size reduction for the same performance. As a metric for the size of bends, we use a box placed around the bend that encompasses the bend structure as well as >99.9% of the input and output waveguide mode power (Figs. 5–7, inset in Fig. 6 for regular bends).

For $\Delta = 7\%$, a throughput efficiency of 98% is achieved with an ATB size of 20 μm (a trench region bend radius of 7 μm), as compared with a regular bend of 80 μm. For $\Delta = 0.7\%$, a reduction from 2.5 mm to an ATB of 96 μm is achieved, with a trench radius of 9 μm. For the lowest Δ of 0.25%, a 180° bend (Fig. 5 inset) was simulated for loss to reduce computational requirements and is representative of the 90° ATB because bend loss is a small part of the total loss (Table II). The 90° ATB field plot in Fig. 5 is given from a simulation with coarse discretization. The lowest index contrast bend is reduced from a 15-mm radius to 250 μm.

Fig. 8 shows the transmission and backscattering power ratio spectra over the C-band communications window of 1530–1570 nm, exhibiting little wavelength dependence as expected, because single-mode coupling is being used through the entire device, and no use is made of either resonance or multimode/path interference. The exception is backscattering in the 180° turn (A), where weak Fabry–Pérot resonances are seen due to the proximity of the input and output waveguides. Markers placed in Fig. 8 at the central wavelength (1550 nm) show the values of transmission and reflection into the fundamental waveguide mode (obtained using overlap integrals). These represent the bend transmission loss values of interest, where 98% was targeted in order to compare the bend sizes. Notably, reflection in all cases is well below −30 dB and, thus, does not present a problem, at least in theoretical design.

A final example is given to illustrate the impact of the cladding taper by removing the portion of the taper in the cladding region in Example B with $\Delta = 0.7\%$ (Fig. 9). A throughput of 69% or a loss of 1.5 dB results in this case.

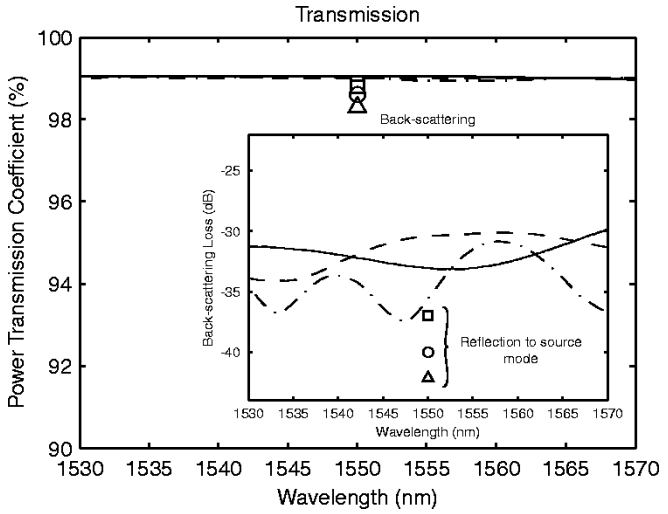

Fig. 8. Transmitted and backscattered power for cases A (dashed–dotted), B (dashed), and C (solid) through the output and input reference planes, respectively. True transmission and reflection into the fundamental mode is shown at the central wavelength (A-triangle, B-circle, C-square).

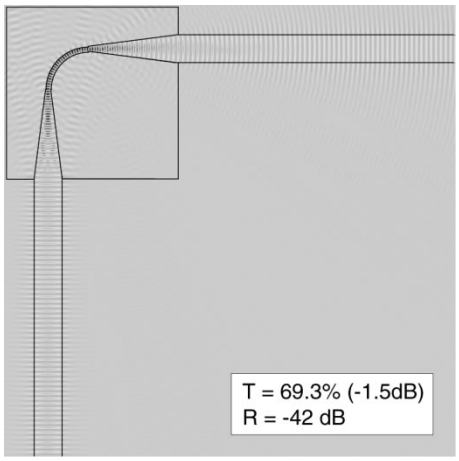

Fig. 9. The ATB from Example B without cladding tapers shows very poor performance. The core taper is virtually lossless, and the loss here is caused by the abrupt junction. No gain results if the core taper is lengthened.

In all of the example cases (A–C), bend size is significantly reduced, most drastically in lower index contrasts, which also have better fiber-chip coupling (i.e., matching to the fiber mode). However, in the vertical (out-of-plane) direction, the aspect ratio of the air trenches for low Δ's may pose fabrication problems.

V. Confinement in the 2-D Cross Section: Effective Indexes, Substrate Loss, Polarization

Here, we present some justification for the use of the EIM in the full structure simulations, and we consider substrate loss and polarization issues, the proper discussion of which requires consideration of the full 2-D cross section of the proposed waveguide structure.

A. Effective Index Versus Exact Modes of the Ideal Air Trench

All 2-D FDTD simulations shown in this paper are carried out using effective indexes for the core, cladding, and air regions

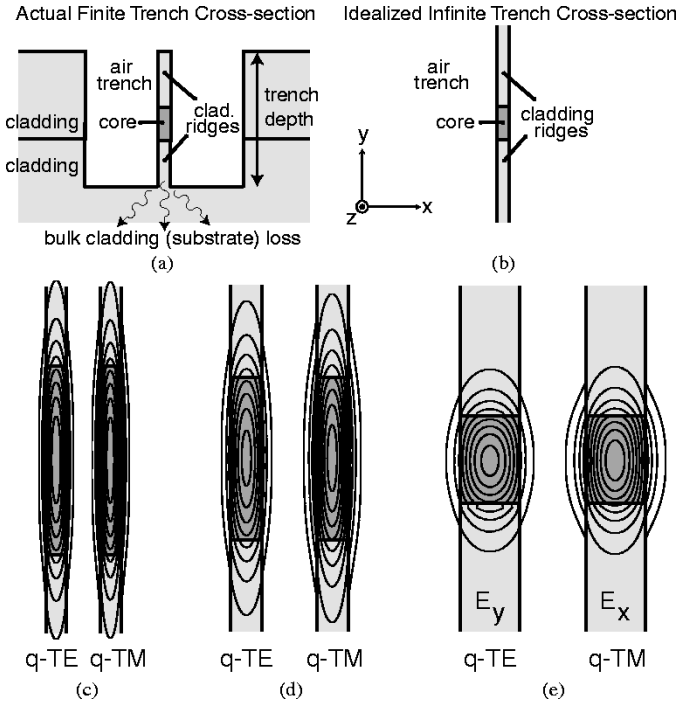

Fig. 10. Schematic of (a) actual air trench cross section and (b) the idealized trench, free of substrate loss. Fundamental quasi-TE and -TM modes of the ideal trench for Examples A–C are in (c)–(e), respectively. Mode plots are to scale individually, but not in proportion to each other. For an idea of relative scale, note that the waveguide width in each of (c)–(e) is the same.

derived for an equivalent 2-D problem using the EIM with perturbation correction [14]. The latter was necessary because air trenches (like rectangular waveguides) cannot be treated using the standard EIM, as is possible for rib waveguides (except to adopt the cladding index as the effective index value in the cladding).

For our simulations, effective indexes are obtained assuming a guided mode and, thus, a waveguide cross- section in which the air trench and cladding regions extend infinitely above and below the core [Fig. 10(b)]. Because the index contrast is much higher in the lateral (x axis in Fig. 10) than in the vertical (y axis) direction, the behavior is very much slablike—confinement is weak in the vertical direction—and the maximum waveguide width for "single modedness" is roughly that of the slab. Having good lateral and poor vertical confinement is acceptable because we are only concerned with making sharp bends in the plane. In fact, allowing poor vertical confinement improves the lateral confinement, although it does present other undesirable properties, such as enhanced substrate loss. The air trench and cladding are in reality of finite vertical extent [Fig. 10(a)], and there will be substrate loss if the modal index is lower than the index of the bulk cladding below the trench. In the case of an ideal air trench of infinite extent, the mode is guided [Fig. 10(b)–(e)].

A vectorial finite-difference mode solver (with metallic-wall boundary conditions placed far from the waveguide) is used to verify the appropriateness of the values obtained through the EIM. Table IV shows a comparison of the modal indexes in the 2-D EIM approximation and from the three-dimensional (3-D) full-vector solver, and Fig. 11 shows the lateral field distributions of the 2-D and 3-D solutions along the x axis for case C,

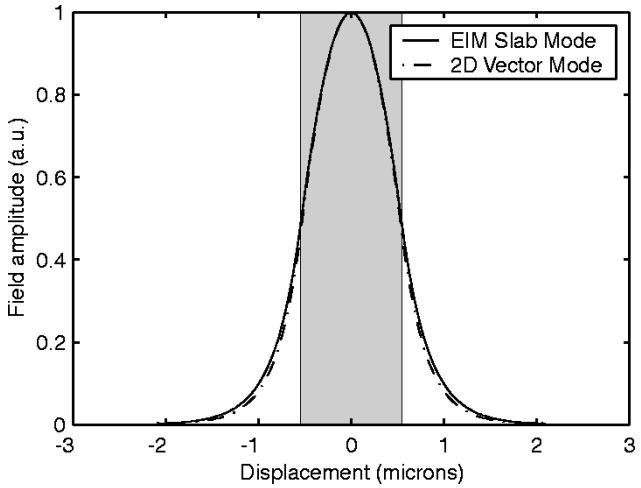

Fig. 11. Comparison of the dominant electric-field component distribution in the horizontal plane at the waveguide axis, as obtained from a vectorial mode solver (dash-dot) and as approximated using the EIM (solid). The EIM field is representative of the 2-D FDTD simulations.

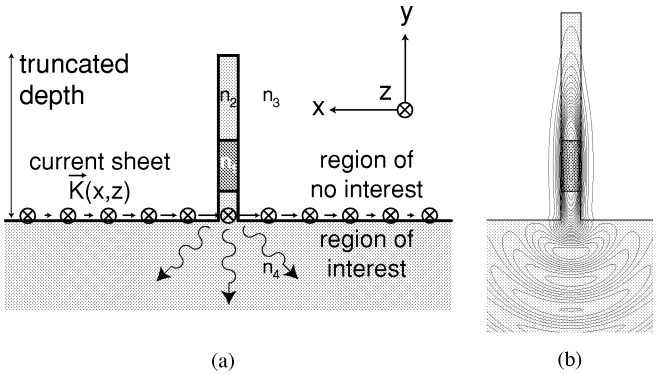

Fig. 12. Calculating substrate loss: (a) Setup of the 2-D equivalent current sheet method (ECSM). (b) Mode solver LM solution example: Real part of the E_y field component for the waveguide of Example B with the bulk cladding 0.6 core heights from the axis.

the worst approximation, according to Table IV. The good match in Fig. 11 provides a justification for the use of the EIM in our 2-D simulations.

B. Polarization Dependence and Loss

The quasi-TE and quasi-TM mode propagation constants in Table IV show that the TM-like mode is more weakly confined and that this structure will not be polarization-independent, especially for tight bend radii [Fig. 10(c)–(e)]. Instead of attempting to compensate for polarization dependence, it is proposed that the real estate savings would justify building two identical circuits (Fig. 2).

Polarization-mode mismatch can hamper the operation of a single polarization device as well by introducing loss, via mode scattering at interfaces. However, in the ATB structure with ideal (vertically infinite, guiding) air trench waveguides, polarization mixing at the interfaces is forbidden by the symmetry of the fields. In an actual ATB, this symmetry is broken at the interfaces by the combination of a substrate layer present below *and* the lateral asymmetry of the leaky bend mode of one of the waveguides. However, in our application, the substrate is kept far enough away to provide low loss, and with it, this coupling term will also be small.

C. Substrate Loss and Minimum Air Trench Depth

In order to curb the substrate loss in the actual ATB [Fig. 10(a)], the air trench must be etched sufficiently deep beneath the core for the evanescent tail of the field to be small where it reaches the bulk cladding. With $n_{\mathrm{mode}} < n_{\mathrm{cladding}}$, the modal field will be oscillatory in the bulk substrate below the trench, and the mode will exhibit leakage through a tunneling process from the core, through the "cladding ridge" beneath it, into the bulk cladding (the field is *evanescent* in the vertical direction in the "ridge"). A deep trench, as demanded here, requires high aspect ratio etching. The mode is weakly confined in the vertical direction, so the air trenches must be several core heights [W_L, Fig. 1(b)] deep for acceptable substrate loss. Since the aspect ratio increases with lower index contrast, fabrication issues will place a lower limit on the index contrast range for which this technique is practical. Making use of the whispering-gallery regime in bending and removing the inner wall of the trench bend completely may ease this difficulty.

It is of interest to evaluate the required depth of the air trench [Fig. 10(a)] given an acceptable substrate loss (much less than total ATB loss). We proceed along two parallel routes to evaluate substrate loss: a semianalytic perturbation method using the mode solution of the ideal (guiding trench) and a numerical, full-vector mode solver for LMs, both taking into consideration the 2-D cross section of the waveguide.

1) 2-D Equivalent Current Sheet Method: We define an equivalent current sheet and use a cylindrical-vector Green's function (e.g., see [9]) approach to evaluate the far-field radiation and, thus, loss per unit length. Since we are interested in small loss, we consider a "perturbative" calculation. That is, ending the air trench at a prescribed depth [Fig. 10(a)] implies a perturbation of the refractive index from the ideal trench [Fig. 10(b)] below that depth. We assume that silica cladding continues below the trench. We also assume that the mode shape remains unperturbed above the air trench-bulk cladding interface and use this field to define an equivalent current sheet just above the bottom of the air trench to represent the fields below [Fig. 12(a), region of interest]. Assuming that the field does not change much in crossing the interface, the current sheet can be moved just below the trench, where we now have a region of uniform index (the bulk cladding or substrate). For a more accurate treatment, we can account for Fresnel reflection due to the interface when translating across it fields that generate the current sheet. A far-field solution of the radiation pattern into the bulk cladding can then easily be calculated integrating a cylindrical-vector Green's function over this source (factoring out first the propagation direction z). A field attenuation coefficient results

$$\alpha = \frac{1}{2}\frac{\left(\frac{dP_{\mathrm{radial}}(z,z_0)}{dz}\right)}{P_{\mathrm{guided}}} \tag{3}$$

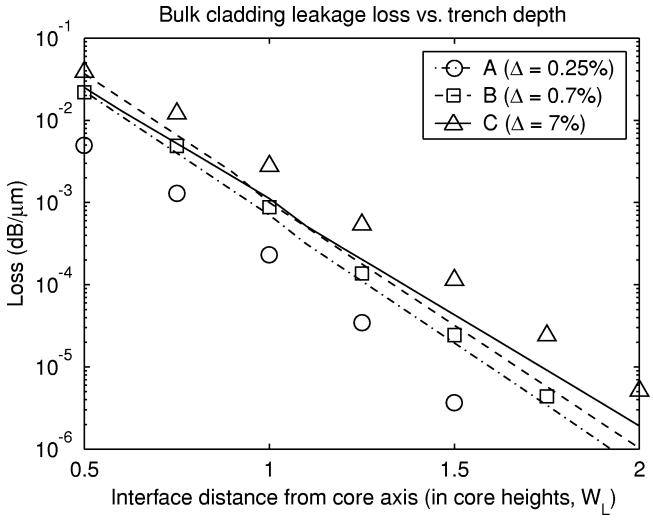

Fig. 13. Bulk cladding loss versus trench etching depth for waveguides of Examples A–C (Figs. 5–7) computed by approximate ECSM (lines) and numerical vector-field mode solver for leaky waveguides (symbols). The discrepancy is due to reflection at the interface with the bulk cladding, not accounted in the ECSM calculation.

where the numerator represents the radial component of far-field radiated power per unit waveguide length, the denominator represents power guided in the mode, and substrate loss is $L_S = -20 \log e^{-\alpha}$ (dB/m).

For air trench waveguide substrate loss calculations, we use the original equivalent current sheet and ignore reflection from the interface, as proper compensation for the reflection on a 2-D interface would complicate the calculation. Normalized 2-D substrate loss results obtained for ATB Examples A–C presented in this paper are shown in lines in Fig. 13, where guided-mode solutions of the ideal air trench waveguide from a vector-field mode solver were used to define the current sheet. From these plots, we choose a trench depth for which the substrate loss is much smaller than the ATB loss of 0.1 dB.

2) Numerical Mode Solver for 2-D Vector Modes: A second set of substrate loss results comes with less physical intuition but with (numerically) exact solutions and is obtained directly from a vectorial mode solver designed for leaky waveguides. We used a staggered vector-field discretization like that in FDTD [17], [18] and implemented PML absorbing boundary conditions in the frequency domain to allow for LMs (e.g., the 1-D example in [19]). The resulting complex eigenvalue problem was solved using a sparse matrix iterative eigenvalue solver (e.g., eigs in MATLAB or ARPACK). The substrate loss results directly from the imaginary part of the mode propagation constant. The computed substrate loss values are plotted in Fig. 13 along with the current sheet results. The discrepancy is attributable to ignored reflection in the the current sheet method. An example modal solution is shown in Fig. 12(b).

For our examples A–C, the mode resembles an air trench mode only within the "air square" [Table IV and Fig. 1(b)], so we take a propagation distance of two "air square" edges for total substrate loss. For a chosen 0.01-dB loss, this gives loss per unit length requirements of 0.00005, 0.00014, and 0.00039 dB/μm for cases A–C, respectively. Total trench depth

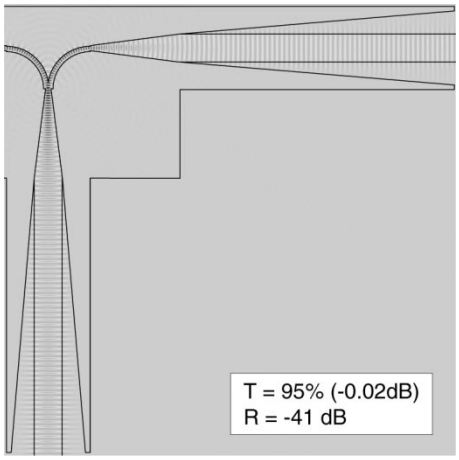

Fig. 14. Simple waveguide tee using ATBs (0.7% index contrast): Dominant E-field component plot from FDTD simulation. Transmission and reflection into source mode given in lower right corner.

[as in Fig. 10(a)] is twice the distance of the trench from the waveguide axis in Fig. 13, if we assume a trench that is symmetric about the core axis but leaks only to the bottom. The loss-per-unit-length values above map onto required normalized trench depth in Fig. 13 (using the mode solver data set). Unnormalizing by the core height W_L from Table IV, we obtain required total trench depths of 24, 15, and 5 μm for Examples A–C. Clearly, a lower index contrast poses greater challenges for fabricating the air trenches but also offers greater reduction in bend size.

Another concern that emerges with the introduction of air trenches is scattering loss, which is common to all high-index contrast structures. We argue that our bends are small enough to have an acceptably low scattering loss. For example, a 20-μm ATB structure (as in case C), assuming a scattering loss of 5 dB/cm, would incur a 0.01-dB total loss due to scattering per 90° bend, as compared with the bending loss of 0.1 dB/bend.

VI. Waveguide Tee Incorporating ATBs

We show as an application a primitive compound structure that makes use of the proposed ATBs, a waveguide T-splitter (90° Y junction). In this structure, additional waveguide offsets at the input bend junction are required for optimal transmission. The field plot and performance are given in Fig. 14. An evenly split, total transmission of 95% is achieved with less than -40-dB reflection to the source. In this example, care was not taken to design for simple fabrication, and the structure's sharp corner at the Y junction would present a problem. An alternative geometry for the power-splitting section, such as a rectangular multimode-interference (MMI) section with outputs wider apart, could be used at the Y junction instead. The intent here was to show compact wide-angle splitting using ATBs. The structure is 180 μm $\times$ 100 μm in size and in the refractive index system of Example B.

VII. Conclusion

By introducing air trenches gradually, away from the core first, in a configuration that allows for adiabatic mode transition

from low to high (trench) index contrast regions, a dramatic reduction in the bending radius of otherwise low-index contrast waveguides is possible without incurring large junction losses through mode mismatch and Fresnel reflection. The "total box size" (effective radius) of a bend was reduced by a factor of 4–60 in our silica examples. Because bending radius is one of the primary factors limiting the density of integration in silica, the use of ATBs, such as the ones presented, may allow dense integration leading to reduced cost and better yield, while preserving the good fiber coupling and propagation loss properties of silica PLCs. We have provided 2-D simulations of example structures with support for this treatment. Arbitrarily low substrate loss is possible to within the limitations on fabricating high aspect ratio trenches, ranging in depth between 5 and 25 μm in our examples. In addition, we suggest that complete removal of the inner wall of the ATB (with necessary modifications to the design) could further improve not only bend loss but also the manufacturability by reducing the vertical structure's aspect ratio. We showed a T-splitter, as a simple compound device using these ATBs.

ACKNOWLEDGMENT

The authors gratefully acknowledge the use of the NPACI Cray T-90 supercomputer at the San Diego Supercomputer Center (SDSC) for all FDTD simulations. Author M. Popović also wishes to thank C. Manolatou for use of her well-written FDTD simulation code and for invaluable and frequent advice and M. J. Khan and M. Watts for fruitful discussions and useful suggestions.

REFERENCES

[1] T. Miya, "Silica-based planar lightwave circuits: Passive and thermally active devices," *IEEE J. Select. Topics Quantum Electron.*, vol. 6, pp. 38–45, Jan. 2000.

[2] E. A. J. Marcatili, "Bends in optical dielectric waveguides," *Bell Syst. Tech. J.*, vol. 48, pp. 2103–2132, Sept. 1969.

[3] M. Heiblum and J. H. Harris, "Analysis of curved optical waveguides by conformal transformation," *IEEE J. Quantum Electron.*, vol. QE-11, pp. 75–83, Feb. 1975.

[4] D. Rowland, "Nonperturbative calculation of bend loss for a pulse in a bent planar waveguide," in *Proc. Inst. Elect. Eng.—Optoelectronics*, vol. 144, Apr. 1997, pp. 91–96.

[5] I. C. Goyal, R. L. Gallawa, and A. K. Ghatak, "Bent planar waveguides and whispering gallery modes: A new method of analysis," *J. Lightwave Technol.*, vol. 8, pp. 768–774, May 1990.

[6] L. H. Spiekman, Y. S. Oei, E. G. Metaal, F. H. Groen, P. Demeester, and M. K. Smit, "Ultrasmall waveguide bends: The corner mirrors of the future?," in *Proc. Inst. Elect. Eng. —Optoelectronics*, vol. 142, Feb. 1995, pp. 61–65.

[7] C. Manolatou, S. G. Johnson, S. Fan, P. R. Villeneuve, H. A. Haus, and J. D. Joannopoulos, "High-density integrated optics," *J. Lightwave Technol.*, vol. 17, pp. 1682–1692, Sept. 1999.

[8] D. Marcuse, *Theory of Dielectric Optical Waveguides*, 2nd ed. Boston, MA: Academic, 1991.

[9] J. A. Kong, *Electromagnetic Wave Theory*. Cambridge, MA: EMW Publishing, 1999.

[10] J. Yamauchi, M. Ikegaya, and H. Nakano, "Bend loss of step-index slab waveguides with a trench section," *Microw. Optical Technol. Lett.*, vol. 5, pp. 251–254, June 1992.

[11] M. K. Smit, E. C. M. Pennings, and H. Blok, "A normalized approach to the design of low-loss optical waveguide bends," *J. Lightwave Technol.*, vol. 11, pp. 1737–1742, Nov. 1993.

[12] E. C. M. Pennings, "Bends in optical ridge waveguides: Modeling and experiments," Ph.D. dissertation, Dept. of Electrical Engineering, Delft University of Technology, Delft, the Netherlands, 1990.

[13] K. Wada, M. Popović, S. Akiyama, H. A. Haus, and J. Michel, "Micron-size bending radii in silica-based waveguides," in *Proc. IEEE/LEOS Summer Topical Meeting WDM Components*, 2001, pp. 13–14.

[14] C. K. Madsen and J. H. Zhao, *Optical Filter Design and Analysis: A Signal Processing Approach*. New York: Wiley, 1999.

[15] G. L. Bona, R. Germann, F. Horst, B. J. Offrein, and H. W. M. Salemink, "Versatile silicon-oxynitride planar lightwave circuits for interconnect applications," in *Proc. 6th Int. Conf. Parallel Interconnects, PI'99*, pp. 145–148.

[16] W. C. Chew, "Electromagnetic theory on a lattice," *J. Appl. Phys.*, vol. 75, pp. 4843–4850, May 1994.

[17] K. Radhakrishnan and W. C. Chew, "An efficient Krylov-subspace-based algorithm to solve the dielectric waveguide problem," *IEEE Trans. Microwave Theory Tech.*, vol. 49, pp. 1345–1348, July 2001.

[18] W. P. Huang, C. L. Xu, W. Lui, and K. Yokoyama, "The perfectly matched layer boundary condition for modal analysis of optical waveguides: Leaky mode calculations," *IEEE Photon. Technol. Lett.*, vol. 8, pp. 652–654, May 1996.

Miloš Popović (S'98) was born in Zaječar, Yugoslavia, in 1977. He received the B.Sc. degree in electrical engineering from Queen's University, ON, Canada, in 1999, and the M.S. degree from the Massachusetts Institute of Technology, Cambridge, in 2002. He is currently working toward the Ph.D. degree, pursuing integrated optics as his research topic.

Kazumi Wada received the B.S. and M.S. degrees and the Ph.D. degree in instrumentation engineering from Keio University, Yokohama, Japan, in 1973, 1975, and 1982, respectively.

Since joining NTT Laboratories, Tokyo, Japan, in 1975, he has been engaged in research on defects in silicon and III–V semiconductor materials and devices, including oxygen precipitation kinetics in Si. From 1981 to 1982, he was a Visiting Scientist at the Massachusetts Institute of Technology (MIT), Cambridge, conducting research on defects in GaAs. From 1982 to 1983, he was a Visiting Specialist at the Science and Technology Agency of the Japanese Government working on establishing a guideline on semiconductor materials research in Japan. Since 1998, he has been with the MIT Microphotonics Center, Department of Materials Science and Engineering, conducting research on silicon-based photonic integrated circuits. His current interest is on-chip optical interconnection for high-speed Si-LSIs. He is author and coauthor of more than 100 refereed journal papers and has edited 13 books. He is an Associate Editor of the *Japanese Journal of Applied Physics*.

Dr. Wada has been serving as Associate Editor of the Institute of Electrical and Electronics Engineers (IEEE)/The Minerals, Metals & Materials Society (TMS) JOURNAL OF ELECTRONIC MATERIALS. He is an active Member of the Materials Research Society, the Electrochemical Society, and the Japan Society of Applied Physics.

Shoji Akiyama received the B.S. and M.S. degrees in chemistry from Kyoto University, Kyoto, Japan, in 1995 and 1997, respectively.

In 1997, he joined Shin-Etsu Handotai (SEH) Company, Ltd. In 2000, he entered Professor L.C. Kimerling's Group at the Department of Materials Science and Engineering, Massachusetts Institute of Technology (MIT), Cambridge.

Hermann A. Haus (S'50–A'55–SM'58–F'62–LF'91) was born in Ljubljana, Slovenia, in 1925. He attended the Technische Hochschule, Graz, and the Technische Hochschule, Vienna, Austria. He received the B.Sc. degree from Union College, Schenectady, NY, in 1949, the M.S. degree from the Rensselaer Polytechnic Institute, Troy, NY, in 1951, and the Sc.D. degree from the Massachusetts Institute of Technology, Cambridge, in 1954.

He joined the Faculty of Electrical Engineering at MIT in 1954, where he is an Institute Professor. He is engaged in research in electromagnetic theory and lasers. He is the author or coauthor of six books and more than 360 journal articles.

Dr. Haus is a Fellow of the American Physical Society and the Optical Society of America (OSA) and a Member of the National Academy of Engineering, the National Academy of Sciences, and the American Academy of Arts and Sciences. He is the recipient of the 1984 Award of the Institute of Electrical and Electronics Engineers (IEEE) Quantum Electronics and Applications Society, the 1987 Charles Hard Townes Prize of the Optical Society of America, the 1990 Outstanding Paper Award of the IEEE TRANSACTIONS ON EDUCATION, the 1991 IEEE Education Medal, the 1994 Frederic Ives Medal of the Optical Society of America, the President's 1995 National Science Medal, the Ludwig Wittgenstein-Preis Award of the Austrian Government 1997, and the Willis E. Lamb Medal, 2001. He holds honorary doctorate degrees from Union College, the Technical University of Vienna, Vienna, Austria, and the University of Ghent, Ghent, Belgium.

Jürgen Michel was educated in Germany and received the degree in physics from the University of Cologne, Cologne, Germany, in 1983, and the Ph.D. degree in applied physics from the University of Paderborn, Paderborn, Germany, in 1987.

He was a Research Scientist at the University of Paderborn. Prior to joining MIT in 1990, he was a Postdoctoral Member of Technical Staff at AT&T Bell Laboratories, studying defect reactions and defect properties in semiconductor materials. Currently, he is a Senior Research Associate in the Microphotonics Center at the Massachusetts Institute of Technology (MIT), Cambridge. He manages and conducts research projects in silicon-based photonic materials and devices and contamination issues in silicon processing. His main focus is currently on optical-clock distribution and coupling and packaging issues in microphotonics and on-chip WDM devices. He is author or coauthor of more than 80 technical articles.